remote sensing

MDPI

Article

Elevation-Dependent Glacier Albedo Modelling Using Machine Learning and a Multi-Algorithm Satellite Approach in Svalbard

Dominik Cyran * and Dariusz Ignatiuk

Faculty of Natural Sciences, Institute of Earth Sciences, University of Silesia in Katowice, Bankowa 12, 40-007 Katowice, Poland; dariusz.ignatiuk@us.edu.pl

* Correspondence: docyran@us.edu.pl

Highlights

What are the main findings?

- Elevation-dependent modelling achieves excellent performance: linear regression (R^2 = 0.84–0.86) for ablation zones where snow–ice transitions dominate, neural networks (R^2 = 0.65) for snow-dominated areas where cumulative thermal history drives albedo evolution.
- Multi-algorithm satellite validation (n = 5) reveals that temporal albedo dynamics are more robustly captured than absolute values, with all algorithms detecting consistent seasonal declines (27.8–35.2%) despite 12% variation in absolute estimates.

What are the implications of the main findings?

- Firstly, a comprehensive comparison of linear vs. non-linear modelling approaches across elevation zones demonstrates that optimal albedo prediction requires recognition of fundamentally different process controls across glacier surfaces, with direct implications for climate sensitivity assessments.
- Validated data-efficient framework requiring only temperature and precipitation from standard AWS installations enables operational application in under-monitored Arctic glacier environments, providing practical tools for real-time albedo forecasting and mass balance projections.

Abstract

Glacier surface albedo controls solar energy absorption and Arctic mass balance, yet comprehensive modelling approaches remain limited. This study develops and validates multiple modelling frameworks for glacier albedo prediction using automatic weather station (AWS) data from Hansbreen and Werenskioldbreen in southern Svalbard during the 2011 ablation season. We compared three point-based approaches across elevation zones. At lower elevations (190 m), linear regression models emphasising snowfall probability or temperature controls achieved excellent performance (R^2 = 0.84–0.86), with snowfall probability contributing 65% and daily positive temperature contributing 86.3% feature importance. At higher elevations (420 m) where snow persists, neural networks proved superior (R^2 = 0.65), with positive degree days (72.5% importance) driving albedo evolution in snow-dominated environments. Spatial modelling extended point predictions across glacier surfaces using elevation-dependent probability calculations. Validation with Landsat 7 imagery and multi-algorithm comparison (n = 5) revealed that while absolute albedo values varied by 12% (0.54–0.60), temporal dynamics showed remarkable consistency (27.8–35.2% seasonal decline). Point-to-pixel validation achieved excellent agreement (mean absolute difference = 0.03 ± 0.02, 5.3% relative error). Spatial validation across

Check for updates

Academic Editor: Hongyi Li

Received: 30 October 2025
Revised: 19 December 2025
Accepted: 24 December 2025
Published: 26 December 2025

Copyright: © 2025 by the authors. Licensee MDPI, Basel, Switzerland. This article is an open access article distributed under the terms and conditions of the Creative Commons Attribution (CC BY) license.

173,133 pixel comparisons demonstrated good agreement (r = 0.62, R^2 = 0.40, RMSE = 0.15), with an accuracy of reproducing temporal evolution within 0.001–0.021 error. These findings demonstrate that optimal glacier albedo modelling requires elevation-dependent approaches combining physically based interpolation with machine learning, and that temporal pattern reproduction is more reliably validated than absolute values. The frameworks provide tools for understanding albedo-climate feedback and improving mass balance projections in response to Arctic warming.

Keywords: glacier albedo; Svalbard; machine learning; linear regression; neural networks; satellite validation; Arctic glaciology

1. Introduction

1.1. Background and Context

Surface albedo represents one of the most critical parameters controlling glacier energy balance and mass loss in the Arctic [1]. As the fraction of incoming solar radiation reflected by glacier surfaces, albedo directly determines the amount of energy available for melting, making it a fundamental driver of glacier response to climate change [2]. Fresh snow exhibits high albedo values (0.8–0.9), while exposed glacial ice reflects significantly less solar radiation (0.3–0.5), creating strong positive feedback mechanisms that can accelerate glacier retreat under warming conditions [3,4].

Arctic glaciers are experiencing rapid changes in response to accelerated warming, with surface albedo feedback playing an increasingly significant role in the evolution of their mass balance [5]. The transition from snow-covered to ice-exposed surfaces during the ablation season creates pronounced temporal and spatial variations in energy absorption, thereby fundamentally altering the sensitivity of glaciers to climate forcing [6]. Beyond this physical transition, biological and geochemical darkening processes have emerged as critical drivers of albedo reduction across Arctic ice masses. While biological darkening processes, including glacier algae proliferation and cryoconite accumulation, have emerged as additional albedo controls on Arctic ice surfaces [7–12], these processes require specialised measurements beyond standard meteorological observations and are not addressed in the present study.

1.2. Study Motivation

Despite the fundamental importance of glacier albedo, current understanding of the processes controlling albedo evolution remains limited, particularly in Arctic environments where complex interactions between temperature, precipitation, and surface conditions create highly variable patterns [13,14]. Satellite observations reveal widespread glacier albedo declines globally [15–17], highlighting the need for robust modelling frameworks to project future changes and understand regional variations in albedo-climate feedback.

Recent advances in machine learning have expanded albedo modelling capabilities, with applications ranging from satellite data assimilation [18] to physics-informed modelling approaches [19–23]. However, the relative performance of different modelling approaches across varying glacier surface conditions remains poorly understood, limiting the development of robust predictive tools for glacier albedo evolution. However, operational albedo monitoring in remote Arctic environments requires approaches that work within typical data constraints of standard AWS installations.

1.3. Research Objectives

Existing physically based albedo models [3,24] require extensive input data that are often unavailable in remote Arctic environments, limiting their practical application on under-monitored glaciers. Initial attempts to apply established albedo parameterisations to Svalbard glaciers yielded unsatisfactory results, likely due to insufficient observational constraints and the complexity of sub-daily processes that cannot be resolved with typical automatic weather station (AWS) measurements [25]. This study, therefore, aims to develop a simplified yet robust modelling framework for glacier albedo prediction that operates within typical data constraints of Arctic field sites [26]—requiring only air temperature from on-glacier AWS and precipitation from nearby meteorological stations.

The primary objectives are to: (1) develop and validate data-efficient albedo models using four key predictors readily available from standard AWS installations: daily positive temperature, snowfall probability, day of year, and positive degree days (PDD) [27]; (2) compare linear regression and neural network approaches [28] to identify optimal model structures for different glacier elevation zones, recognising that ablation-dominated and accumulation-dominated environments may require different modelling strategies; (3) extend point-based predictions across entire glacier surfaces through spatial modelling that incorporates elevation-dependent snowfall probability calculation using temperature lapse rates [29] and orographic precipitation corrections [30]; and (4) validate spatial model predictions against independent Landsat-derived albedo estimates [31] to assess model accuracy under real-world application scenarios.

This pragmatic approach prioritises model simplicity and data availability over process complexity [32], recognising that robust predictions with limited input data are more valuable for operational glaciology than complex models requiring unavailable observations. The resulting framework is designed to be transferable to other data-limited Arctic glacier environments where comprehensive energy balance measurements are impractical.

2. Study Area

The study focuses on two glaciers located in southern Svalbard: Hansbreen and Werenskioldbreen. Both glaciers are situated on the western coast of Spitsbergen, the largest island of the Svalbard archipelago, within the high Arctic climate zone. Regional climate conditions are characterised by maritime Arctic features due to the moderating influence of oceanic currents, with considerable interannual and seasonal variability [33,34]. The area experiences distinctive radiation regimes influenced by the high latitude location, with incoming solar radiation strongly modified by topographic shading, atmospheric attenuation, and complex albedo-elevation relationships that significantly affect the glacier's energy balance [35,36]. The research was conducted in proximity to the Polish Polar Station Hornsund, which provides logistical support for glaciological and meteorological studies in the region [37,38].

Hansbreen (77°04′N, 15°38′E) is a ~16 km long tidewater glacier with a current area of approximately 52 km^2, representing a significant decrease from earlier estimates due to ongoing retreat [39,40]. The glacier exhibits a polythermal structure with both temperate and cold ice zones, influenced by its meridional orientation, which impacts radiation receipt and ablation patterns along its north–south flowing profile [41,42]. The glacier terminates in Hornsund fjord and has been subject to extensive glaciological research since the 1980s, including detailed studies of ablation modelling and surface energy balance [42,43].

Werenskioldbreen (77°05′N, 15°23′E) is a land-terminated glacier covering approximately 25.7 km^2 and extending about 9.5 km in length, showing notable area reduction from 27.1 km^2 in 2008 [44]. This valley-type glacier displays polythermal characteristics with complex thermal structure variations, and its roughly east–west orientation creates

distinct radiation exposure conditions that influence its mass balance regime differently than the north–south trending Hansbreen [44,45]. Both glaciers have experienced significant changes in recent decades, making them important indicators of Arctic climate change [46,47].

3. Data and Methods

3.1. Data Sources

3.1.1. Automatic Weather Station Data

Observational data were obtained from three automatic weather stations (AWS) deployed on the study glaciers. Two stations were located on Hansbreen: AWS_H4 at approximately 190 m and AWS_H9 at approximately 420 m, while one station was positioned on Werenskioldbreen (AWS_WRN) at approximately 380 m.

Surface albedo was measured using Kipp & Zonen CMP3 pyranometers (ISO 9060:2018 Class C, Kipp & Zonen B.V., Delft, The Netherlands [48]) measuring downwelling and upwelling shortwave radiation following World Meteorological Organisation (WMO) and Global Cryosphere Watch standards, with measurement uncertainty of ± 0.03 for daily albedo values [44]. Each AWS was equipped with temperature-measuring devices, allowing calculation of positive degree days (PDD) and daily temperatures at the stations.

Additional meteorological data were sourced from the Polish Polar Station Hornsund, located in proximity to the study glaciers [49]. Key variables included precipitation amounts, which were essential for calculating snowfall probability and served as a key predictor variable in the albedo models [50]. The study utilised multi-annual data from 2010 to 2012 to provide comprehensive temporal coverage for model development and validation. The primary dataset for model development comprised measurements from the 2011 season (8 April to 4 September), when solar elevation angles in Hornsund exceeded 20 degrees above the horizon throughout the period, ensuring reliable albedo measurements. Data from Hansbreen stations for 2010 and Werenskioldbreen for 2012 were utilised for model training and validation purposes, providing temporal variability and independent datasets for assessing model performance across different meteorological conditions and glacier surface states.

3.1.2. Satellite Data

Landsat 7 Enhanced Thematic Mapper Plus (ETM+) imagery was acquired for two cloud-free dates during the 2011 study period: 26 July and 20 August [51]. These images provided spatial albedo estimates for model validation across the entire glacier surface. The satellite data were processed using both single-algorithm and multi-algorithm approaches through Google Earth Engine [52].

3.1.3. Digital Elevation Models

30 m resolution Digital Elevation Models (DEMs) from ArcticDEM were used to provide topographic context and enable spatial interpolation of meteorological variables across the glacier surfaces [53]. The DEMs covered the complete extent of both Hansbreen (~52 km^2) and Werenskioldbreen (~25.7 km^2) glacier areas with vertical accuracy of ± 0.5 m and horizontal accuracy of ± 3 m according to ArcticDEM specifications. Data were accessed on 27 September 2024, through the Polar Geospatial Center data portal. The DEMs facilitated the calculation of elevation-dependent lapse rates for temperature extrapolation across the altitudinal range of 0–852 m, for the study area.

3.1.4. Missing Data Treatment

Data gaps at AWS_WRN (17% of 2011 season, approximately 25 days) resulted from equipment malfunctions that were concentrated mostly in late April. Missing data were handled using context-dependent approaches:

Observational statistics (Section 4.1, Table 1):

Missing periods were excluded from all calculations. Mean albedo (0.80 ± 0.03), temperature statistics (mean: 0.1 ± 0.1 °C, range: −9.1 to 8.7 °C), and data coverage percentage (83%) were computed only from available observations. This conservative approach prevents interpolation artefacts from biassing reported observational statistics.

Model training and validation:

Missing data were gap-filled using forward-fill interpolation (last observation carried forward, LOCF method). Previous valid observations for temperature and albedo were maintained until the next measurement, and derived variables (PDD, daily positive temperature) were recalculated from gap-filled temperature values. This approach ensures temporal continuity required for model validation while preserving observed patterns before and after data gaps.

The late April timing of data gaps (before peak ablation) and the stability of meteorological conditions during this period minimise potential impacts on model performance at AWS_WRN.

3.2. Albedo Calculation and Modelling Approach

3.2.1. AWS-Based Albedo Calculation

Surface albedo (α) was calculated from AWS pyranometer measurements using the standard formula [3]:

$$\alpha = R_{_upwelling}/R_{_downwelling} \quad (1)$$

where $R_{_upwelling}$ is the downward-facing solar radiation sensor, and $R_{_downwelling}$ is the upward-facing solar radiation sensor, both measured in W m^{-2}.

3.2.2. Snowfall Probability Calculation

A statistical model was developed to estimate snowfall probability based on meteorological conditions, combining temperature data from glacier automatic weather stations with precipitation data from the Hornsund station, following approaches established for Arctic environments [27]. The model incorporated temperature-based probability using a sigmoid function around the freezing point and precipitation-based probability with logarithmic scaling. Orographic corrections were applied to account for elevation differences between the Hornsund precipitation station and glacier AWS locations, using a precipitation gradient correction of 19% per 100 m elevation gain as established for Svalbard water balance calculations by Nowak & Hodson [54].

The temperature-based snowfall probability was calculated as:

$$P_{_temp} = 1/(1 + \exp(1.5 \times (T - 1.0))) \quad (2)$$

where T is air temperature in °C.

Precipitation probability used a piecewise function: trace precipitation (0–0.1 mm) received a base probability of 0.2, while measurable precipitation ($\geq$0.1 mm) was scaled logarithmically from 0.1 mm to 5.0 mm for maximum probability. The final snowfall probability was calculated as the product of temperature and precipitation probabilities. This combined approach yields snowfall probability values ranging from 0 (no precipitation and warm temperatures) to 1 (heavy precipitation and freezing temperatures), with typical ablation-season values ranging from 0.05 to 0.45 across the elevation gradient.

3.2.3. Linear Regression Models

Multiple linear regression models were developed to predict surface albedo using meteorological and temporal variables, following established approaches in glacier modelling [1]. The feature set included day of year (seasonal patterns), air temperature, positive degree days (cumulative thermal forcing), and calculated snowfall probability. Models were trained using data from 2010 and 2012, with 2011 data reserved for independent validation.

Two primary modelling approaches were implemented:

1. Snowfall-dominated model: Emphasising snowfall probability as the primary predictor
2. Temperature-dominated model: Focusing on daily positive temperature as the main driver

3.2.4. Neural Network Approach

A Multi-Layer Perceptron (MLP) neural network was implemented to test for non-linear relationships between meteorological variables and albedo, using the scikit-learn framework [55]. The network architecture consisted of hidden layers with 100 and 50 neurons, ReLU activation functions, and L2 regularisation to prevent overfitting. Feature standardisation was applied to optimise training convergence.

There were also other modelling approaches tested (XGBoost, Random Forest), but they underperformed and therefore are not presented in this study.

3.3. Spatial Albedo Modelling

3.3.1. Meteorological Variable Interpolation

Meteorological variables measured at point locations (AWS) were spatially interpolated across the entire glacier surface using elevation-dependent lapse rates. Temperature interpolation employed a lapse rate of -0.53 °C per 100 m elevation, consistent with regional studies from Svalbard [56]. Other variables were interpolated using elevation-based linear functions derived from the station measurements.

3.3.2. Grid-Based Albedo Prediction

The trained linear regression models were applied to spatially interpolated meteorological grids to generate wall-to-wall albedo maps for both glaciers. Modelled albedo maps were made for the satellite image acquisition dates (26 July and 20 August 2011) to enable direct comparison with remotely sensed albedo estimates.

3.4. Satellite Albedo Calculation

3.4.1. Single-Algorithm Approach

Broadband albedo was calculated from Landsat 7 surface reflectance data using the raster calculator expression provided in the manuscript. This approach utilised weighted combinations of spectral bands to estimate integrated shortwave albedo across the 0.3–3.0 μm wavelength range (visible to near-infrared solar spectrum) [57].

The implemented formula was:

$$\alpha = 0.356 \times \text{Band2} + 0.130 \times \text{Band3} + 0.373 \times \text{Band4} + 0.085 \times \text{Band5} + 0.072 \times \text{Band7} - 0.0018 \quad (3)$$

where Band2 through Band7 represent the surface reflectance values from Landsat 7 ETM+ spectral bands [51]: Band 2 (blue: 0.45–0.52 μm), Band 3 (green: 0.52–0.60 μm), Band 4 (red: 0.63–0.69 μm), Band 5 (near-infrared: 0.77–0.90 μm), and Band 7 (shortwave infrared: 2.09–2.35 μm).

3.4.2. Point-to-Pixel Satellite-AWS Comparison

Direct validation of satellite-derived albedo was performed through point-to-pixel comparison at the three automatic weather station locations. AWS coordinates were verified using GPS measurements and field documentation. Satellite albedo values were extracted from the Landsat-derived albedo rasters at the pixel corresponding to each AWS location. Daily mean AWS albedo values (24 h averages) were used for comparison to maintain methodological consistency with the daily temporal resolution employed throughout the manuscript for albedo modelling and analysis. Verification showed that the difference between daily mean albedo and instantaneous albedo at the specific satellite overpass times was marginal (<0.04), falling within combined measurement uncertainty (±0.06–0.08). This minimal discrepancy reflects the midday timing of satellite acquisitions when albedo is most stable, and the limited diurnal albedo variation during the 24 h daylight of the Svalbard ablation season.

3.4.3. Multi-Algorithm Approach

Five broadband albedo algorithms were implemented using Landsat 7 ETM+ Surface Reflectance imagery (Collection 2, Level 2) via Google Earth Engine: Liang (2001) [57], Tasumi et al. (2008) [58], Silva et al. (2016) [59], Simple visible-NIR, and Knap et al. (1999) [60]. Surface reflectance data (atmospherically corrected) were retrieved for 26 July and 20 August 2011, with quality masking applied to remove clouds and cloud shadows using the QA_PIXEL band.

To ensure data quality and physical consistency, pixel-level filtering excluded values outside physically realistic ranges for glacier surfaces (albedo < 0.15 representing rock/debris/water; albedo > 0.85 indicating cloud contamination or sensor artefacts), consistent with thresholds applied in previous Landsat-based glacier albedo studies. The filtering range was validated through manual inspection of glacier masks to verify appropriate exclusion of non-glacial features while retaining legitimate albedo extremes. This approach retained 89–97% of glacier pixels across all scenes and dates, confirming minimal loss of valid data. Mean albedo was calculated over the glacier boundaries for each algorithm, providing both individual glacier and combined system statistics. The Knap et al. algorithm [60], specifically calibrated for glacier surfaces using Landsat TM bands, was designated as the primary reference algorithm.

3.5. Training and Validation Strategy

The modelling framework employed a multi-year temporal validation approach to ensure robust performance assessment across varying meteorological conditions. Training datasets comprised 2010 measurements from Hansbreen stations (AWS_H4 and, AWS_H9) and 2012 measurements from Werenskioldbreen (AWS_WRN). The 2011 ablation season data (8 April to 4 September, 149 days) from AWS_H4, AWS_H9 and AWS_WRN were reserved exclusively for independent temporal validation and did not participate in model training.

Linear regression models were trained using data from both lower elevation (AWS_H4) and higher elevation (AWS_H9) stations on Hansbreen 2010 data plus AWS_WRN on Werenskioldbreen 2012 data, to capture the full range of elevation-dependent albedo dynamics. The neural network (MLP) was trained specifically using AWS_H9 2010 data because this station represents snow-dominated high-elevation conditions where persistent snow cover throughout the ablation season creates non-linear albedo evolution patterns. Lower elevation stations (AWS_H4, AWS_WRN) experience complete snow removal and binary snow–ice transitions that are effectively captured by linear approaches.

Spatial validation employed an independent dataset: Landsat 7 imagery from 26 July and 20 August 2011. These satellite observations were used exclusively for validating spatial model predictions across entire glacier surfaces and did not participate in model training or temporal validation. Point-to-pixel comparisons at AWS locations provided additional independent verification of satellite retrieval accuracy before broader spatial validation analysis.

This multi-scale validation strategy ensures that model performance is assessed against both temporal dynamics (AWS time series) and spatial patterns (satellite imagery) using fully independent datasets.

4. Results

4.1. Observed Albedo Variations

4.1.1. Temporal Evolution of Meteorological Conditions

The 2011 ablation season showed typical maritime Arctic characterised by high temporal variability in both temperature and precipitation patterns. All Hansbreen AWS recorded 149 days of data during the extended season (8 April–4 September), providing comprehensive coverage of albedo evolution from winter snow cover through peak ablation to early autumn snow accumulation. The Werenskioldbreen AWS had intermittent data gaps due to equipment malfunction (Table 1).

4.1.2. Temperature

AWS_H4 recorded the longest melt season with 101 days of daily mean temperatures above 0 °C (67.8% of the season). Daily mean temperatures averaged 0.4 ± 0.1 °C across the entire study period, with extremes ranging from −7.8 ± 0.1 °C (16 May) to 7.8 ± 0.1 °C (17 August). The seasonal temperature evolution showed characteristic Arctic patterns: rapid spring warming beginning in early May, peak summer temperatures in July–August averaging 5.2 ± 0.1 °C, and gradual autumn cooling with first sustained freezing occurring in early September (Table 1) (Figure 1).

AWS_H9 experienced 83 days above 0 °C (55.7% of the season), reflecting its higher elevation position. Mean daily temperatures averaged −0.6 ± 0.1 °C, with a range from −11.6 ± 0.1 °C (8 April) to 5.1 ± 0.1 °C (23 August). The elevation difference of 230 m between AWS_H4 and AWS_H9 created a mean temperature gradient of 0.4 °C per 100 m, consistent with typical Arctic lapse rates during the ablation season (Table 1) (Figure 1).

AWS_WRN recorded 81 days above 0 °C (54.0% of the season) despite data gaps due to equipment malfunctions. Available measurements showed mean daily temperatures of 0.1 ± 0.1 °C, with extremes from −9.1 ± 0.1 °C (19 May) to 8.7 ± 0.1 °C (16 August). The station exhibited greater temperature variability than expected based purely on elevation, likely reflecting local topographic influences and different exposure characteristics (Table 1) (Figure 1).

4.1.3. Precipitation and Snowfall Probability

The Hornsund precipitation record [49] showed 73 days with measurable precipitation (≥0.1 mm) during the study period, totalling 184 mm across the ablation season. Significant precipitation events (>5 mm/day) occurred on 18 days, with the largest single-day total of 23.4 mm recorded on 15 June. The precipitation pattern showed characteristic maritime Arctic features: frequent light precipitation events throughout the season, episodic heavy precipitation, and a mix of precipitation types even during the summer months.

Snowfall probability calculations revealed marked elevation-dependent patterns. AWS_H4 showed snowfall probabilities > 0.5 on 34 days (23% of the season), concentrated in spring and autumn periods. AWS_H9 exhibited much higher snowfall potential with

probabilities > 0.5 on 67 days (45% of the season), including several mid-summer events during cold precipitation episodes. AWS_WRN showed intermediate behaviour with 48 days (36% of the season) exceeding 0.5 probability, reflecting its transitional elevation position.

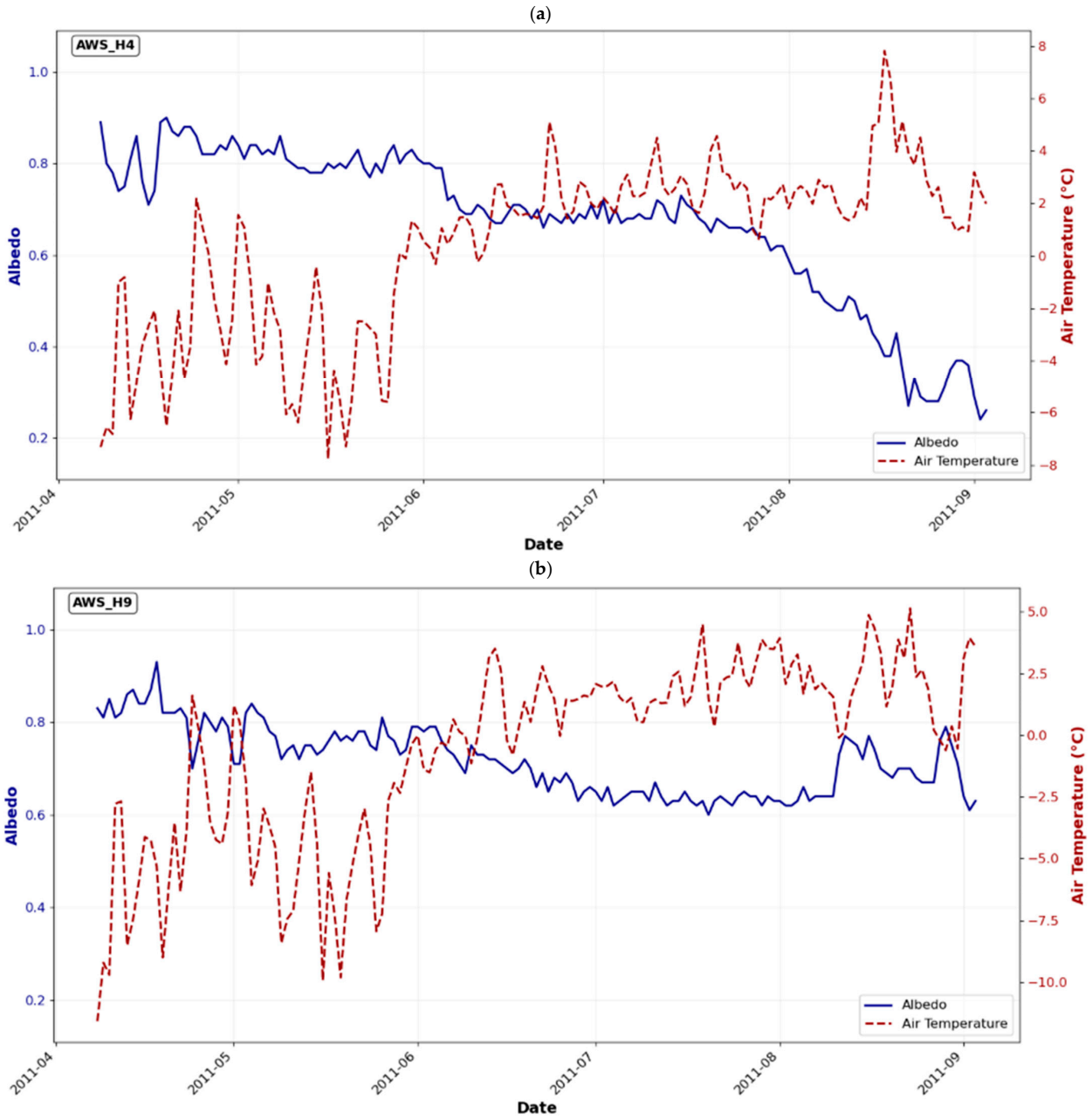

Figure 1. *Cont.*

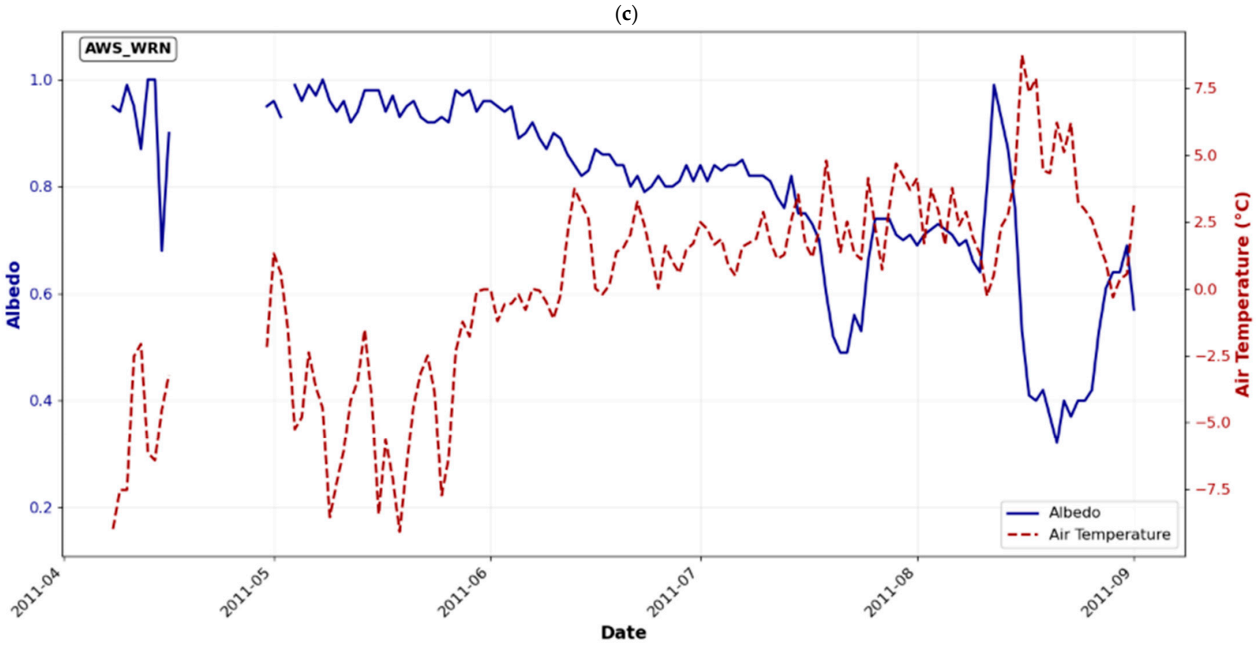

Figure 1. Temporal evolution of daily mean albedo and temperature during the 2011 ablation season (8 April–4 September) at three automatic weather stations: (**a**) AWS_H4 (190 m), (**b**) AWS_H9 (420 m), and (**c**) AWS_WRN (380 m). Blue lines show albedo, red dashed lines show air temperature.

4.1.4. Seasonal Albedo Dynamics

Station-Specific Patterns:

AWS_H4 demonstrated the most pronounced seasonal albedo evolution, with values declining from early season highs of 0.89 ± 0.03 to minimum values of 0.24 ± 0.03 by early September, representing the complete transition from snow to bare ice (Figure 1a). Mean albedo across the entire season was 0.67 ± 0.03. The station enabled extensive ice exposure through its long melt season. Distinct seasonal phases were observed: spring snow cover maintenance (April–May, mean albedo 0.82 ± 0.03), rapid transition period (June–July, declining from 0.80 ± 0.03 to 0.65 ± 0.03), and stable ice exposure (August–September, mean albedo 0.35 ± 0.03). The most rapid albedo decreases occurred during sustained warm periods, with the lowest values (0.24 ± 0.03) recorded on 2 September following peak summer temperatures (Table 1) (Figure 1).

AWS_H9 maintained consistently higher albedo values throughout the season, with a mean albedo of 0.72 ± 0.03. The seasonal evolution was more gradual than AWS_H4, declining from winter values of 0.93 ± 0.03 to minimum values of 0.60 ± 0.03 during peak summer (20 July) (Figure 1b). AWS_H9 never experienced complete snow removal, maintaining persistent snow/firn cover throughout the ablation season. Maximum daily average temperatures reached only 5.1 ± 0.1 °C (23 August), insufficient to cause complete ice exposure (Table 1) (Figure 1).

AWS_WRN exhibited distinctly different behaviour, with a mean albedo of 0.80 ± 0.03 calculated from available measurements. The station maintained the highest albedo values among all sites despite its intermediate elevation (Figure 1c). The station showed extreme seasonal variability, ranging from a maximum value of 1.00 ± 0.03 (13 April) to a minimum value of 0.32 ± 0.03 (21 August). Notable features included maintaining a very high albedo (>0.95) through early May, a gradual decline from June to July, dramatic decreases during the warmest period in mid-August, when daily average temperatures reached 8.7 ± 0.1 °C (16 August), and a rapid recovery following fresh snowfall events. The station exhibited a few data gaps due to equipment malfunctions, mainly during the period in late April (Table 1) (Figure 1).

Table 1. Summary statistics of meteorological conditions and albedo observations at AWS stations during the 2011 ablation season (8 April–4 September).

Data Coverage (%)	Albedo Range	Mean Albedo	Days > 0 °C	Temp Range (°C)	Mean Temp (°C)	Elevation (m)	Station
100	0.24–0.90	0.67 ± 0.03	101 (67.8%)	−7.8 to 7.8 ± 0.1	0.4 ± 0.1	190	AWS_H4
100	0.60–0.93	0.72 ± 0.03	83 (55.7%)	−11.6 to 5.1 ± 0.1	−0.6 ± 0.1	420	AWS_H9
83	0.32–1.00	0.80 ± 0.03	81 (54.0%)	−9.1 to 8.7 ± 0.1	0.1 ± 0.1	380	AWS_WRN

4.2. Linear Regression Model Performance

4.2.1. Overall Model Validation

The snowfall-probability-dominated linear regression model achieved excellent predictive performance, with an overall R^2 of 0.74 and RMSE of 0.08 across the independent 2011 validation dataset (AWS_H4 and AWS_WRN) (Table 2). The model successfully captured 74% of the variance in observed albedo using four predictor variables: day of year, daily temperature, positive degree days, and snowfall probability. Model uncertainty, quantified by residual standard deviation, was 0.10.

Table 2. Model performance comparison for different albedo prediction approaches.

Key Finding	AWS_H9 R^2	AWS_WRN R^2	AWS_H4 R^2	RMSE	R^2	Training Data	Primary Features	Model Type
Best for ablation zones with snowfall events	-	0.57	0.84	0.08	0.74	2010 AWS_H4 AWS_H9 2012 AWS_WRN	Snowfall probability (65.0%)	Linear (Snowfall)
Temperature dominates ablation zones	-	0.62	0.86	0.08	0.77	2010 AWS_H4 AWS_H9 2012 AWS_WRN	Daily positive temp (86.3%)	Linear (Temperature)
Best for snow/firn-dominated surfaces	0.65	-	-	0.04	0.65	2010 AWS_H9 only	Positive degree days (72.5%)	Neural Network (MLP)

Feature importance analysis revealed snowfall probability as the dominant predictor (65% relative importance), followed by air temperature (24%), positive degree days (6%), and seasonal patterns (5%) (Table 2). The strong dominance of snowfall probability validates the conceptual framework that fresh snow accumulation is the primary driver of albedo variations on Arctic glaciers during the ablation season. The overall performance statistics are dominated by ablation-zone conditions, which covered the vast majority of both glaciers during the 2011 melt season.

4.2.2. Station-Specific Performance

Model performance varied significantly between stations (Table 2, Figure 2a,b). AWS_H4 showed exceptional performance (R^2 = 0.84, RMSE = 0.07), indicating that the linear regression approach effectively captured albedo dynamics at this lower elevation site where snow–ice transitions dominate surface conditions. The model successfully reproduced both gradual seasonal decline and rapid fluctuations associated with snowfall events.

AWS_WRN demonstrated moderate performance (R^2 = 0.57, RMSE = 0.10), indicating a greater complexity in albedo dynamics at this site. The lower performance likely results from data gaps and periodical local extreme meteorological effects (supra-glacial stream near the AWS).

4.2.3. Alternative Modelling Approaches

The temperature-dominated linear regression model achieved superior overall performance (R^2 = 0.77, RMSE = 0.08) when daily positive temperature was emphasised as the primary predictor (Figure 2c,d). Model uncertainty (residual standard deviation)

was 0.10, identical to the snowfall-dominated approach. This approach showed thermal processes accounting for 95.8% of predictive importance, with daily positive temperature contributing 86.3% and positive degree days contributing 9.5%, compared to only 0.2% for precipitation processes (Table 2). Station-specific performance was excellent at AWS_H4 (R^2 = 0.86, RMSE = 0.06) and good at AWS_WRN (R^2 = 0.62, RMSE = 0.09) (Figure 2c,d).

The neural network approach (Multi-Layer Perceptron) achieved good performance (R^2 = 0.65, RMSE = 0.04) with lower uncertainty (residual standard deviation = 0.03) using a single-station analysis at AWS_H9 (Table 2). The model converged in 175 training iterations. Importance analysis revealed positive degree days as the dominant feature (72.5% importance), followed by seasonal patterns (26.8%), while air temperature and snowfall probability showed minimal importance (1.4% combined). This indicates that cumulative thermal history, rather than instantaneous conditions, drives albedo patterns at higher elevation sites, where snow and firn do not melt completely during the season and there is no exposure of glacial ice (Figure 2e).

(**a**)

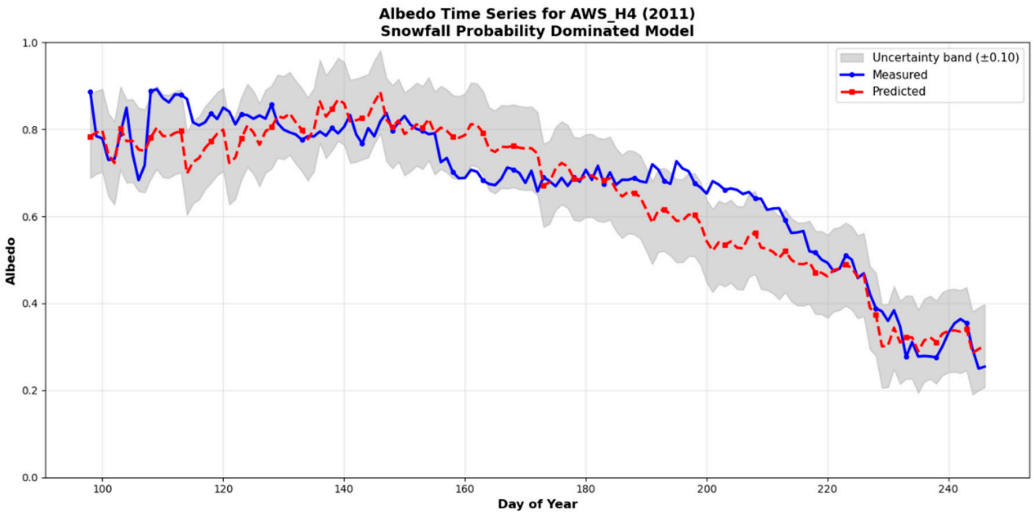

(**b**)

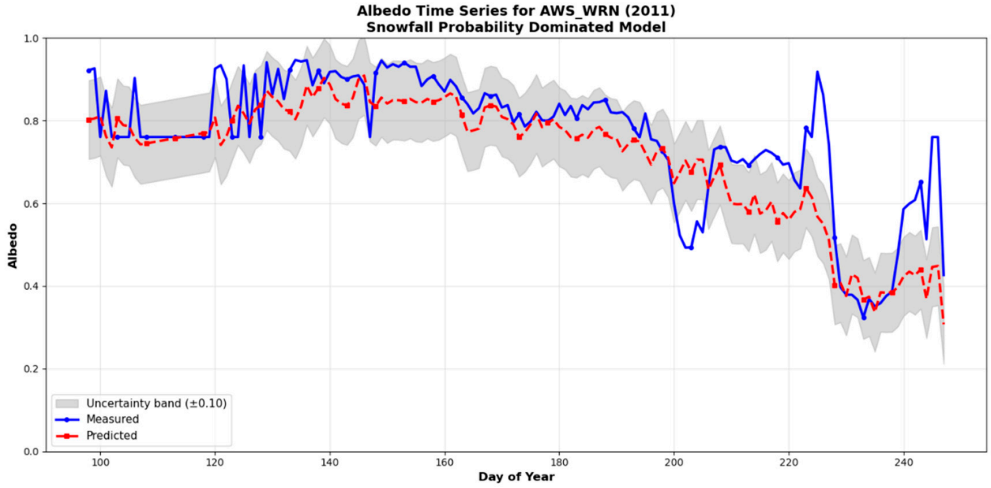

Figure 2. *Cont.*

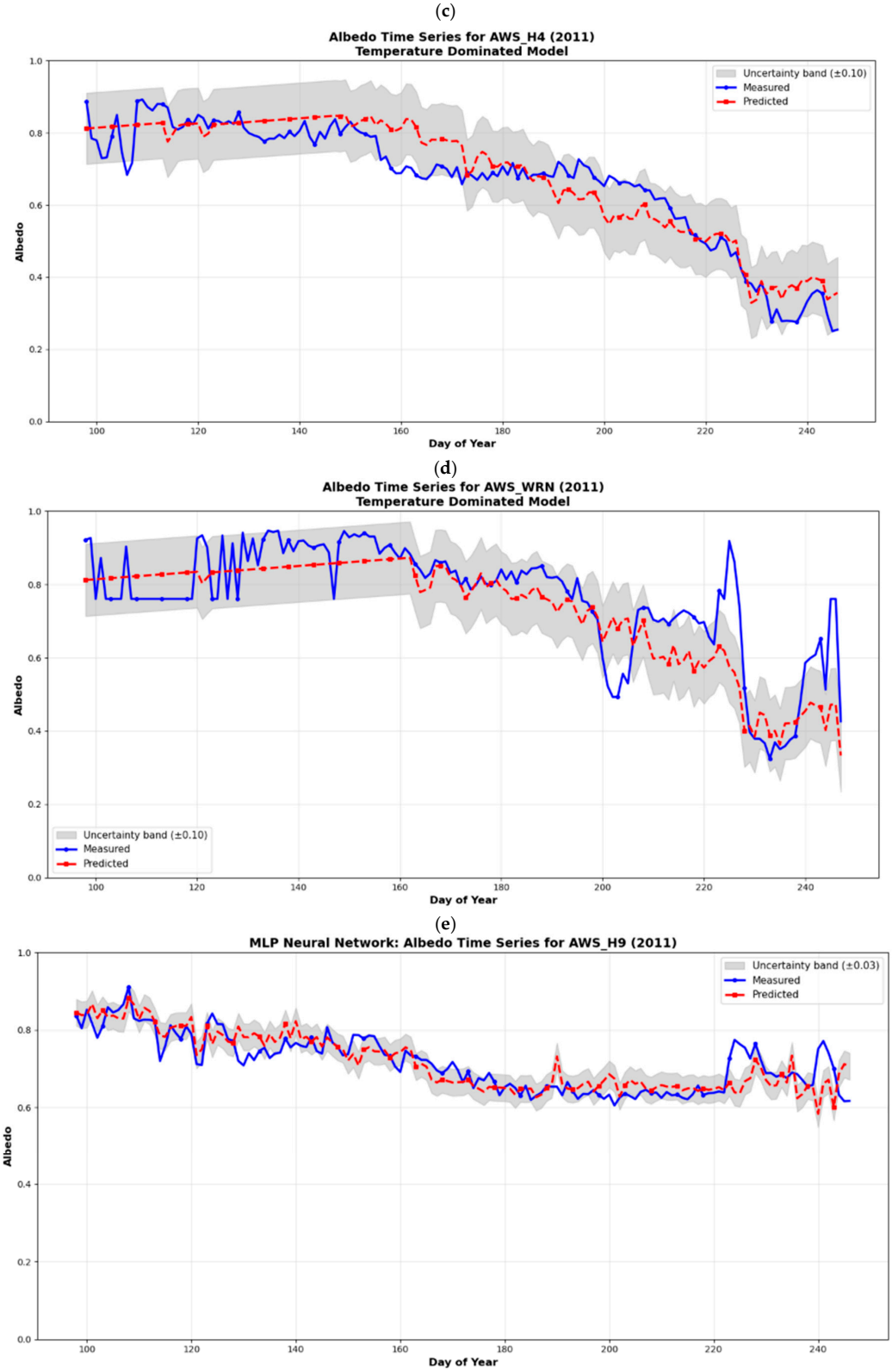

Figure 2. Time series validation at individual stations showing measured versus predicted albedo evolution, with seasonal pattern reproduction for linear (**a**,**b**) snowfall probability dominated, (**c**,**d**) temperature dominated) and non-linear (**e**) approaches.

4.3. Spatial Albedo Model Results

4.3.1. Spatial Modelling Approach

A spatial albedo modelling approach was implemented: a snowfall-dominated model with elevation-dependent snowfall probability calculation. The model utilised glacier-specific AWS stations (AWS_H4 for Hansbreen, AWS_WRN for Werenskioldbreen) and incorporated temperature lapse rates (−0.53 °C/100 m) to extend point-based AWS measurements across entire glacier surfaces.

4.3.2. Snowfall-Dominated Model Results

The snowfall-dominated model calculated snowfall probability at each grid point using local temperature and orographically corrected precipitation following the methodology described in Section 3.2.2 (Equation (2)). Temperature was adjusted for elevation using the lapse rate (−0.53 °C/100 m) as described in Section 3.3.1, and precipitation correction applied the orographic factor of 19% per 100 m elevation gain [54].

For 26 July 2011, the model predicted a mean albedo of 0.62 ± 0.03 for Hansbreen and 0.68 ± 0.03 for Werenskioldbreen (Figure 3a,b). Snowfall probability fields ranged from 0.02 to 0.29 (mean 0.14) for Hansbreen and 0.00–0.33 (mean 0.05) for Werenskioldbreen. Predicted albedo ranged from 0.57 to 0.67 ± 0.03 for Hansbreen and 0.62–0.76 ± 0.03 for Werenskioldbreen.

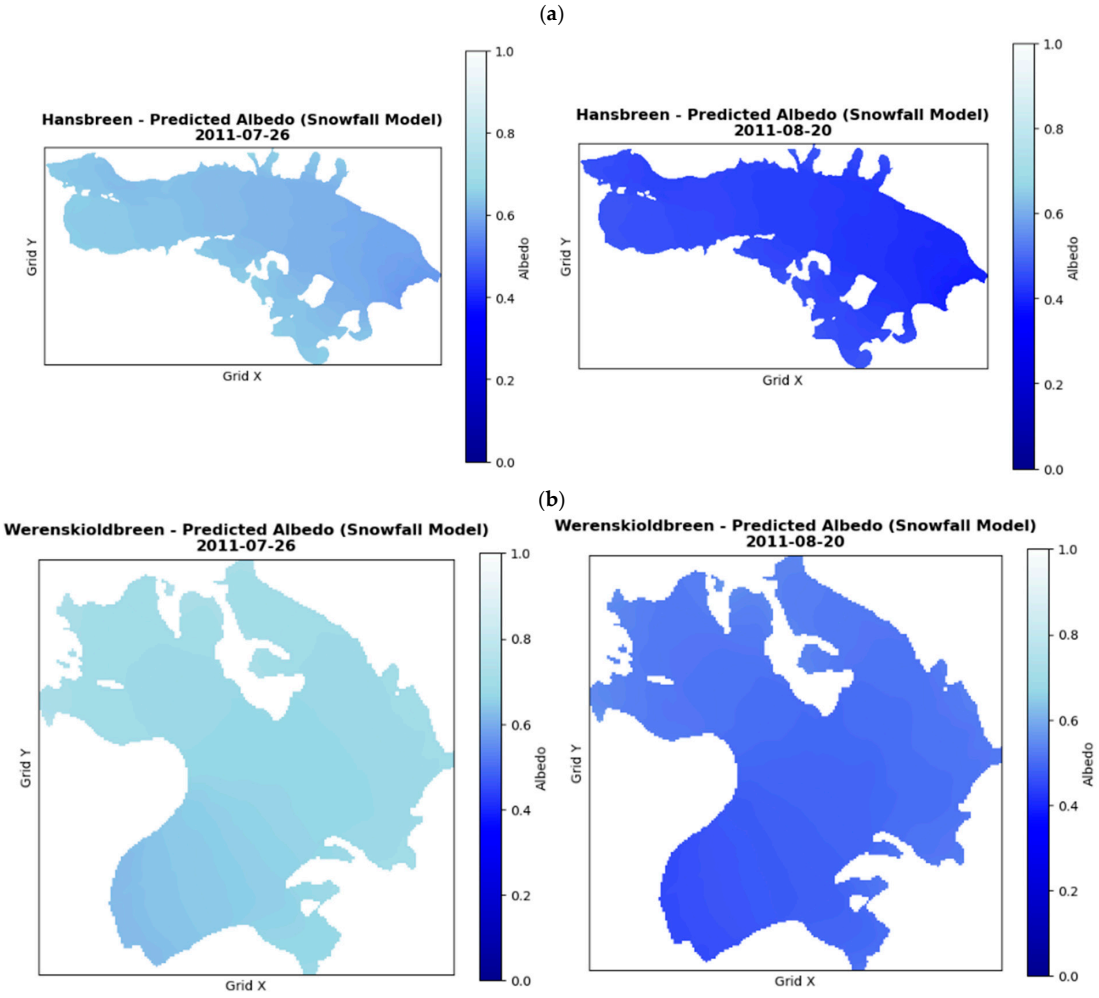

Figure 3. Spatial albedo predictions for 26 July and 20 August 2011: Snowfall-dominated model (elevation-dependent probability) for Hansbreen (**a**) and Werenskioldbreen (**b**).

For 20 August 2011, the mean albedo was 0.44 ± 0.03 for Hansbreen and 0.50 ± 0.03 for Werenskioldbreen (Figure 3a,b). Snowfall probability was zero across both glaciers (0.00 mean). Temperature probability ranged from 0.00 to 0.12 for Hansbreen and 0.00–0.23 for Werenskioldbreen. Predicted albedo ranged from 0.39 to 0.50 ± 0.03 for Hansbreen and 0.45–0.58 ± 0.03 for Werenskioldbreen. Temporal albedo declines from July to August were 0.18 for both glaciers (Table 3).

Table 3. Spatial albedo predictions from the snowfall-dominated model.

Temporal Change	Range	Mean Albedo	Glacier	Date	Model Type
-	0.57–0.67	0.62 ± 0.03	Hansbreen	26 July	Snowfall (Elev-Dep)
-	0.62–0.76	0.68 ± 0.03	Werenskioldbreen	26 July	Snowfall (Elev-Dep)
−0.18	0.39–0.50	0.44 ± 0.03	Hansbreen	20 August	Snowfall (Elev-Dep)
−0.18	0.45–0.58	0.50 ± 0.03	Werenskioldbreen	20 August	Snowfall (Elev-Dep)

4.3.3. Spatial Patterns

The model showed elevation-dependent albedo gradients across both glaciers. Albedo values increased systematically from the terminus regions to the upper accumulation areas. For Hansbreen (elevation range 17–715 m), July albedo increased from 0.57 ± 0.03 at lower elevations to 0.67 ± 0.03 at higher elevations. For Werenskioldbreen (elevation range 67–852 m), July albedo increased from 0.62 ± 0.03 to 0.76 ± 0.03 across the elevation range.

By August, albedo ranges were 0.39–0.50 ± 0.03 for Hansbreen and 0.45–0.58 ± 0.03 for Werenskioldbreen. The snowfall-dominated model produced spatially varying snowfall probability fields (July: 0.02–0.29 for Hansbreen, 0.00–0.33 for Werenskioldbreen).

4.4. Satellite-Based Albedo

4.4.1. Multi-Algorithm Satellite Albedo Analysis

Comparison of five broadband albedo algorithms revealed systematic differences in absolute values but consistent temporal patterns (Table 4). After quality filtering to exclude rock/debris (albedo < 0.15) and cloud contamination (albedo > 0.85), algorithm-specific mean albedo values ranged from 0.54 Liang algorithm [57]) to 0.60 (Knap et al. algorithm [60], representing a 12% range in absolute values.

All algorithms detected substantial temporal decreases between 26 July and 20 August 2011. Hansbreen experienced albedo decreases of 27.8–34.6% (absolute: −0.20 to −0.25), while Werenskioldbreen showed similar decreases of 30.0–35.2% (absolute: −0.21 to −0.24). Quality filtering retained 88.8–96.5% of glacier pixels, confirming minimal cloud contamination over the study areas despite high scene-wide cloud cover (61–70%).

The Knap et al. glacier-specific algorithm [60] produced moderate absolute values and the smallest relative temporal changes (27.8% for Hansbreen, absolute −0.20, 33.2% for Werenskioldbreen, absolute −0.23). Initial high albedo values in late July (0.69–0.73) indicated predominantly snow-covered surfaces, while August values (0.47–0.51) suggested extensive exposed glacier ice, reflecting advanced summer melt conditions.

Table 4. Multi-algorithm satellite albedo comparison for Hansbreen, Werenskioldbreen, and the combined system, 26 July and 20 August 2011.

Relative Change (%)	Absolute Change	20 August Albedo	26 July Albedo	Algorithm
(−32.3 ± 2.7)	(−0.23 ± 0.02)	(0.47 ± 0.04)	(0.70 ± 0.03)	Hansbreen
−34.3	−0.22	0.43	0.65	Liang [57]

Table 4. *Cont.*

Relative Change (%)	Absolute Change	20 August Albedo	26 July Albedo	Algorithm
−33.7	−0.22	0.44	0.66	Tasumi et al. [58]
−31.1	−0.22	0.51	0.73	Silva et al. [59]
−34.5	−0.25	0.48	0.73	Simple visible-NIR
−27.8	−0.2	0.51	0.71	Knap et al. [60] *
(−32.7 ± 2.2)	(−0.23 ± 0.02)	(0.45 ± 0.03)	(0.68 ± 0.02)	Werenskioldbreen
−34.9	−0.23	0.42	0.65	Liang [57]
−34.3	−0.22	0.44	0.66	Tasumi et al. [58]
−30	−0.21	0.48	0.69	Silva et al. [59]
−35.2	−0.24	0.45	0.69	Simple visible-NIR
−33.2	−0.23	0.47	0.7	Knap et al. [60] *
(−31.9 ± 2.9)	(−0.22 ± 0.02)	(0.47 ± 0.03)	(0.69 ± 0.03)	Combined System
−34.5	−0.22	0.43	0.65	Liang et al. [57]
−33.9	−0.22	0.44	0.66	Tasumi et al. [58]
−31.2	−0.22	0.5	0.72	Silva et al. [59]
−35.1	−0.25	0.47	0.72	Simple visible-NIR
−29.5	−0.21	0.5	0.71	Knap et al. [60] *

* Glacier-specific algorithm. Quality filtering (0.15 < albedo < 0.85) retained 89–97% of pixels. The Combined System represents the area-weighted average of both glaciers.

4.4.2. Point-to-Pixel Validation at AWS Locations

A direct comparison between the daily mean AWS albedo and satellite-derived albedo at the three AWS locations is presented in Table 5. For 26 July 2011, absolute differences ranged from 0.04 (AWS_H4, AWS_WRN) to 0.07 (AWS_H9), corresponding to relative differences of 5.4% to 10.8%. For August 20, 2011, absolute differences ranged from 0.00 (AWS_H4) to 0.03 (AWS_WRN), representing relative differences of 0.0% to 8.1%.

AWS_H4 showed absolute differences of 0.04 on 26 July and 0.00 on 20 August. AWS_H9 exhibited an absolute difference of 0.07 on 26 July and 0.01 on 20 August. AWS_WRN showed absolute differences of 0.04 on 26 July and 0.03 on 20 August.

The mean absolute difference across all six comparisons was 0.03 ± 0.02, with a mean relative difference of 5.3 ± 3.9%. All observed differences fell within the combined measurement uncertainty range of ±0.06–0.08 albedo units (AWS uncertainty ±0.03; satellite uncertainty ±0.05).

Table 5. Point-to-pixel comparison between daily mean AWS albedo and Landsat-derived albedo at automatic weather station locations.

Relative Difference (%)	Absolute Difference	Satellite Albedo	AWS Albedo (Daily Mean)	AWS Station	Time (UTC)	Date
6.1	0.04	0.62 ± 0.05	0.66 ± 0.03	AWS_H4	11:40	26 July 2011
10.8	0.07	0.72 ± 0.05	0.65 ± 0.03	AWS_H9	11:40	26 July 2011
5.4	0.04	0.70 ± 0.05	0.74 ± 0.03	AWS_WRN	11:40	26 July 2011
0	0	0.35 ± 0.05	0.35 ± 0.03	AWS_H4	11:30	20 August 2011
1.5	0.01	0.67 ± 0.05	0.68 ± 0.03	AWS_H9	11:30	20 August 2011
8.1	0.03	0.34 ± 0.05	0.37 ± 0.03	AWS_WRN	11:30	20 August 2011

4.4.3. Landsat-Derived Albedo Estimates

Landsat 7 imagery provided independent albedo estimates for model validation on 26 July and 20 August 2011. Satellite-derived mean albedo values were 0.63 ± 0.11 and 0.45 ± 0.18 for Hansbreen, and 0.62 ± 0.13 and 0.43 ± 0.20 for Werenskioldbreen on the respective dates (Table 6) (Figure 4a,b). Realistic albedo filtering (0.15–0.85 range) removed 2.4–13.7% of pixels to exclude non-glacial surfaces, including water, rock, debris, and sensor errors, with greater filtering needed for the August images.

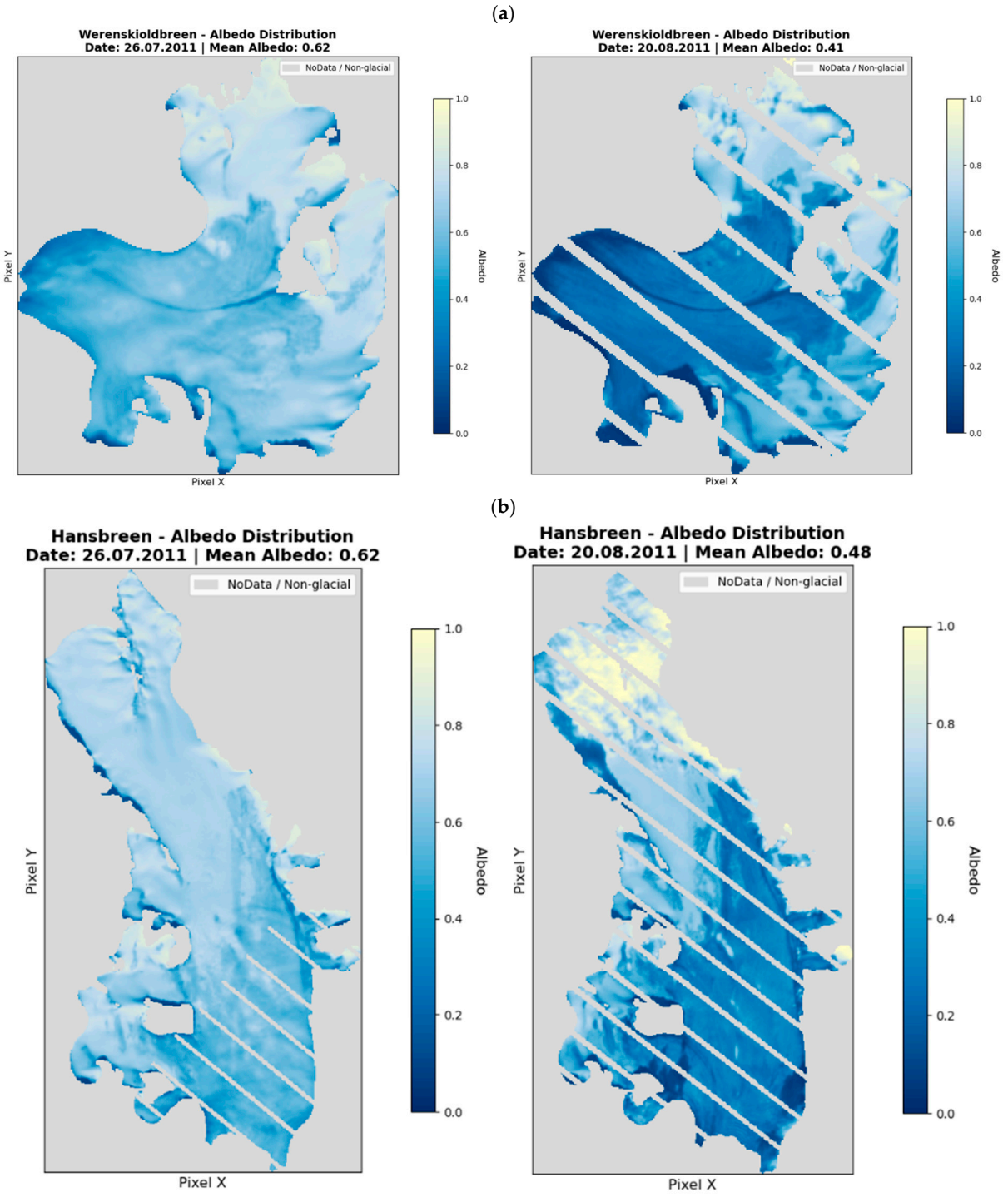

Figure 4. Satellite albedo validation for snowfall-dominated spatial model: (**a**,**b**) Landsat-derived albedo maps for 26 July and 20 August 2011.

Table 6. Satellite albedo validation results for snowfall-dominated spatial model compared to Landsat-derived albedo estimates. Both spatial modelling approaches (snowfall-dominated and temperature-dominated) produced similar results; the snowfall-dominated model is presented here.

Bias	NRMSE (%)	RMSE	R^2	r	Model Mean ± SD	Satellite Mean ± SD	Pixels	Date	Glacier
−0.006	16.4	0.1	0.26	0.51	0.62 ± 0.03	0.63 ± 0.11	67,658	26 July	Hansbreen
−0.007	38	0.17	0.38	0.61	0.44 ± 0.03	0.45 ± 0.18	54,259	20 August	Hansbreen
0.056	20.8	0.13	0.4	0.63	0.67 ± 0.03	0.62 ± 0.13	28,603	26 July	Werenskioldbreen
0.077	45.7	0.2	0.55	0.74	0.50 ± 0.03	0.43 ± 0.20	22,613	20 August	Werenskioldbreen
+0.030 ± 0.043	30.2 ± 13.9	0.15 ± 0.04	0.40 ± 0.12	0.62 ± 0.10	-	-	173,133	-	Overall

The satellite estimates showed strong temporal consistency with AWS observations, capturing substantial albedo decreases between July and August. Observed temporal changes of −0.18 (Hansbreen) and −0.19 (Werenskioldbreen) from satellite data aligned closely with spatial modelling approaches developed in this study (Section 4.3). Given the similar performance of both spatial modelling approaches (snowfall-dominated and temperature-dominated; see Section 4.3), validation was conducted using the snowfall-dominated model with elevation-dependent probability calculation.

4.4.4. Model-Satellite Comparison

Direct pixel-by-pixel comparison between the snowfall-dominated model and satellite-derived albedo revealed good spatial agreement (Table 6). Overall correlation coefficients were 0.62 ± 0.09, with R^2 values of 0.40 ± 0.12 across 173,133 pixel comparisons spanning both glaciers and dates. Root mean square error averaged 0.15 ± 0.04, representing 30.2 ± 13.9% normalised error relative to mean satellite albedo values.

Glacier-specific performance showed Werenskioldbreen (r = 0.68, R^2 = 0.47) outperforming Hansbreen (r = 0.56, R^2 = 0.32). The spatial model showed minimal systematic bias overall (+0.030), though with contrasting patterns between glaciers: Hansbreen exhibited near-zero bias (−0.006 to −0.007), while Werenskioldbreen showed moderate positive bias (+0.056 to +0.077), indicating slight overestimation, particularly during peak ice exposure in August.

Spatial agreement was stronger for August conditions (R^2 = 0.38–0.55) compared to July (R^2 = 0.26–0.40), contrasting with expectations that heterogeneous late-summer surfaces would be more challenging to model. The model excelled at reproducing temporal albedo evolution, with predicted seasonal changes of −0.18 (Hansbreen) and −0.18 (Werenskioldbreen) matching observed satellite changes of −0.18 and −0.19, respectively, yielding temporal change errors of only 0.001–0.021.

5. Discussion

5.1. Elevation-Dependent Albedo Controls

The contrasting performance of linear versus non-linear models across elevation zones reveals fundamental differences in the physical processes controlling glacier albedo [1,3]. Linear regression models achieved excellent performance at lower elevation sites (AWS_H4: R^2 = 0.84–0.86; AWS_WRN: R^2 = 0.57–0.62) where complete snow removal exposes glacial ice during peak ablation. At these locations, albedo variations follow predictable relationships with meteorological forcing [23]. The binary nature of snow–ice transitions creates straightforward relationships that linear models effectively capture.

Two linear approaches showed comparable performance: the snowfall-dominated model (R^2 = 0.74) with snowfall probability contributing 65% importance and the temperature-dominated model (R^2 = 0.77) with daily positive temperature contributing 86.3% importance. This apparent duality reflects the coupled nature of albedo controls—thermal processes drive underlying seasonal decline through snow removal, while precipitation events create rapid albedo increases that temporarily override thermal forcing [24]. Both modelling approaches successfully captured these dynamics at ablation-dominated sites.

In contrast, the neural network approach proved superior at the snow-dominated, higher-elevation site (AWS_H9: R^2 = 0.65), where linear models performed poorly. The dominance of positive degree days (72.5% importance) indicates that cumulative thermal history, rather than instantaneous conditions, drives albedo evolution in persistent snow environments. Complex processes, including snow metamorphism, grain size evo-

lution, and subsurface energy transfer, require non-linear modelling approaches in these settings [13,28].

These findings directly address the research objectives outlined in Section 1.3, demonstrating that data-efficient models using only temperature and precipitation can achieve robust performance while remaining practical for operational Arctic glacier monitoring.

5.2. Spatial Modelling Performance

The spatial modelling approach (snowfall-dominated) produced remarkable predictions. This convergence validates the robustness of the elevation-dependent interpolation framework using temperature lapse rates [29,56] and suggests that both thermal and precipitation processes must be represented for accurate spatial predictions, regardless of which is emphasised.

Point-to-pixel validation at AWS locations demonstrated excellent satellite retrieval accuracy, with a mean absolute difference of 0.03 ± 0.02 (5.3 ± 3.9% relative difference) between daily mean AWS albedo and Landsat-derived estimates (Table 5). All observed differences fell within combined measurement uncertainty (±0.06–0.08 albedo units), providing confidence in satellite-based validation [61,62].

The multi-algorithm satellite albedo comparison (Table 4) reveals an important consideration for glacier albedo validation studies. While absolute albedo values varied by up to 12% across the five tested algorithms (range: 0.54–0.60), all algorithms demonstrated remarkable consistency in capturing temporal dynamics, with relative temporal changes varying by only 7% (27.8–35.2% seasonal decline). This finding indicates that algorithm selection primarily affects absolute calibration rather than the ability to detect albedo evolution patterns. The glacier-specific Knapet al. [60] algorithm produced intermediate absolute values and the most conservative temporal change estimates (27.8–33.2%), suggesting it provides a balanced reference for validation in Arctic glacier environments. The high pixel retention rates after quality filtering (88.8–96.5%) across all algorithms confirm the robustness of the realistic albedo range filtering approach (0.15–0.85) for separating glacial surfaces from rock, debris, and cloud contamination. These results emphasise that while multi-algorithm approaches are valuable for assessing absolute albedo uncertainty, single well-calibrated glacier-specific algorithms are sufficient for validating temporal albedo dynamics in modelling studies. Future satellite validation efforts should prioritise temporal consistency over absolute accuracy, particularly when assessing model performance in capturing seasonal albedo evolution.

Pixel-by-pixel comparison between modelled and satellite-derived albedo revealed good spatial agreement across 173,133 comparisons ($r = 0.62$, $R^2 = 0.40$, RMSE = 0.15). The model excelled at reproducing temporal albedo evolution, with predicted seasonal changes matching observed satellite changes within an error range of 0.001–0.021. Observed albedo decreases of −0.18 between 26 July and 20 August 2011, were accurately captured by the modelling approach, demonstrating the framework's capability for capturing dynamic albedo processes [22].

Spatial agreement was stronger for August conditions ($R^2 = 0.38$–0.55) compared to July ($R^2 = 0.26$–0.40), contrary to expectations that heterogeneous late-summer surfaces would be more challenging to model. This pattern likely reflects the clearer elevation-dependent gradients in ice-exposed surfaces compared to patchy snow conditions earlier in the season [62].

5.3. Implications for Glacier Mass Balance

The observed magnitude of seasonal albedo decline (up to 0.66 at AWS_H4) quantifies the strength of positive feedback mechanisms in Arctic glacier systems [4,5]. Lower albedo

surfaces absorb more incoming solar radiation, which accelerates melting and further reducing albedo in a self-reinforcing cycle. The elevation-dependent nature of this feedback creates spatially heterogeneous energy inputs that significantly influence the glacier-wide mass balance's sensitivity to climate warming [62].

The dominance of thermal processes in ablation zones (86.3% importance in the temperature-dominated model) indicates high sensitivity to Arctic warming. Even moderate temperature increases will shift the elevation threshold for persistent snow cover upward, thereby expanding areas that experience complete snow removal and low albedo conditions [16]. This process amplification will accelerate glacier mass loss beyond the direct effects of increased sensible heat flux.

The success of snowfall probability modelling (65% importance) validates the critical role of precipitation timing in controlling glacier albedo [14]. Fresh snow can dramatically increase surface albedo from ice values (~0.3) to snow values (~0.8), temporarily reversing positive feedback cycles. However, sustained thermal forcing ultimately overwhelms precipitation effects, particularly as warming reduces snowfall frequency and accelerates snow removal even following precipitation events [15,17].

Given that Svalbard experienced a temperature increase of approximately 1.5–2.0 °C over recent decades, our findings suggest that the elevation threshold for snow-dominated conditions (currently ~400–500 m) may have shifted upward by 150–200 m, expanding the area subject to complete ice exposure and associated albedo feedback by approximately 10–15% of glacier area.

5.4. Methodological Considerations and Limitations

The systematic positive bias in spatial predictions (+0.030 overall, ranging from −0.006 for Hansbreen to +0.077 for Werenskioldbreen) suggests the elevation-dependent interpolation approach may not fully capture local surface heterogeneity and microclimate effects. The reduced performance at topographically complex sites suggests that processes such as wind redistribution, shadowing, and variable exposure necessitate more sophisticated spatial treatment beyond simple lapse rate approaches [32].

Beyond the statistical limitations discussed above, our models also omit important physical processes that influence spatial albedo patterns. A significant limitation not captured by our models is wind-driven snow redistribution, particularly prevalent at Hansbreen, where prevailing easterly winds cause substantial snow transport from east to west across the glacier surface [35,63]. This redistribution creates complex spatial patterns of snow accumulation and ablation that cannot be represented by elevation-dependent interpolation alone, potentially contributing to the observed spatial biases and reduced model performance in topographically exposed areas.

Several limitations constrain the generalizability of results. The analysis is based on a single ablation season (2011), which may not represent the full range of meteorological variability encountered across multiple years. The spatial scope is limited to two glaciers in southern Svalbard, and transferability to more continental Arctic environments or different latitude bands remains to be validated [26]. The 17% data loss at Werenskioldbreen due to equipment malfunctions may have influenced model performance assessments.

Satellite validation was limited by the constrained temporal coverage, with only two cloud-free acquisition dates available during the study period. This limitation prevented assessment of model performance across a broader range of atmospheric and surface conditions [64]. The realistic albedo filtering approach (0.15–0.85 range) successfully removed non-glacial contamination but may also exclude legitimate extreme values in very dark ice or fresh snow surfaces.

5.5. Practical Recommendations

Based on these findings, we recommend the following approach for glacier albedo modelling:

For ablation-dominated areas (typically <400–500 m elevation in Svalbard-like climates): Use linear regression approaches, emphasising either temperature or snowfall probability predictors. These areas undergo complete snow removal and experience binary snow–ice transitions, which linear models effectively capture (R^2 = 0.84–0.86).

For snow-dominated areas (typically at elevations above 400–500 m): Implement neural networks or other non-linear approaches that capture cumulative thermal history effects. Positive degree days emerge as the critical predictor in these environments (72.5% importance).

For spatial applications: Implement elevation-dependent modelling strategies rather than uniform approaches. Both snowfall-dominated and temperature-dominated spatial models yield similar results when properly calibrated, providing flexibility based on the available data.

5.6. Future Research Directions

Critical priorities include extending temporal validation to multiple years to test model stability and identify potential non-stationarity in albedo-climate relationships. Multi-year validation is essential to assess whether the elevation-dependent modelling framework remains valid under different climatic conditions.

Spatial scaling to additional Svalbard glaciers and other Arctic regions would test model transferability and enable regional albedo projections [47]. Comparative studies across different Arctic regions (Alaska, Greenland, and the Canadian Arctic) would establish the broader applicability of the elevation-dependent framework.

Integration of albedo modelling with glacier mass balance and ice dynamics models would enable comprehensive assessment of climate change impacts [19,20]. Coupled modelling approaches could quantify the relative importance of albedo feedback versus other climate forcing mechanisms in determining glacier response to warming scenarios, potentially incorporating physics-informed AI approaches for improved computational efficiency [21].

6. Conclusions

This study demonstrates that optimal glacier albedo modelling requires elevation-dependent approaches that recognise fundamentally different process controls across glacier surfaces. Linear regression models excel in ablation-dominated environments (R^2 = 0.84–0.86) where binary snow–ice transitions create predictable albedo dynamics, with thermal processes (86.3% importance) and snowfall probability (65% importance) as dominant controls. Conversely, neural networks prove superior in snow-dominated areas (R^2 = 0.65) where cumulative thermal history effects (72.5% importance) require non-linear modelling.

Spatial modelling achieved good agreement with satellite observations across 173,133 pixel comparisons (r = 0.62, R^2 = 0.40, RMSE = 0.15), with excellent temporal accuracy capturing observed albedo decreases of −0.18 to −0.19 within 0.001–0.021 error. Point-to-pixel validation demonstrated satellite retrieval accuracy within a 5.3% relative difference from AWS measurements. The snowfall-dominated spatial approach produced satisfying results, validating the robustness of elevation-dependent interpolation frameworks.

The multi-algorithm satellite validation demonstrated that temporal albedo dynamics are more robustly captured than absolute values, with all five tested algorithms detecting consistent seasonal declines (27.8–35.2%) despite 12% variation in absolute albedo esti-

mates. This finding validates the reliability of satellite-based temporal validation for glacier albedo models and suggests that model assessment should prioritise temporal pattern reproduction over absolute value matching, particularly given the inherent uncertainties in both satellite retrievals and ground-based measurements.

The contrasting behaviour between linear and non-linear albedo controls suggests that glacier response to climate change may involve threshold effects and discontinuous transitions rather than gradual linear responses. Understanding and predicting these non-linear behaviours will be essential for reliable glacier projections, particularly as Arctic warming may push glacier systems across critical process thresholds.

This research advances glacier albedo modelling through several key contributions. First, it demonstrates that optimal modelling approaches depend critically on glacier surface conditions, with linear methods excelling in ablation zones and non-linear approaches required for snow-dominated environments. This finding challenges one-size-fits-all modelling frameworks and suggests that elevation-dependent modelling strategies may significantly improve predictive accuracy.

Second, the study validates the effectiveness of temperature-precipitation-based snowfall probability calculations for Arctic glacier applications. The strong correlation between calculated snowfall probability and observed albedo variations ($r = 0.406$ at AWS_H9) provides an objective method for incorporating precipitation timing and phase effects into predictive models without requiring direct snowfall measurements.

Third, the comprehensive comparison between point-based AWS measurements, spatial model predictions, and satellite observations establishes a robust validation framework for glacier albedo studies. The realistic albedo filtering approach (0.15–0.85 range) successfully removes non-glacial contamination while preserving legitimate extreme values, providing a practical solution for quality control in satellite-based glacier monitoring.

The research also contributes to understanding albedo-climate feedback mechanisms in Arctic glacier systems. The observed magnitude of seasonal albedo decline (up to 0.66 at lower elevations) quantifies the strength of positive feedback processes, while elevation-dependent patterns reveal the spatial heterogeneity of climate sensitivity across glacier surfaces.

The observed seasonal albedo decline (up to 0.66) quantifies strong positive feedback mechanisms that will amplify Arctic glacier response to warming. The methods and findings presented here are directly applicable to other Arctic glacier regions, supporting broader applications in glacier monitoring and climate impact assessment. The elevation-dependent modelling framework provides a transferable approach for capturing spatial heterogeneity in albedo processes, while the validation methodology offers standardised procedures for satellite-based glacier albedo monitoring.

Future research should focus on developing hybrid modelling approaches that combine the predictive accuracy of linear methods in ablation zones with the process representation capabilities of non-linear approaches in snow-dominated environments. Physics-informed neural networks offer promising avenues for incorporating energy balance constraints while maintaining flexibility to capture complex process interactions.

Author Contributions: Conceptualization, D.C. and D.I.; methodology, D.C. and D.I.; software, D.C.; validation, D.C. and D.I.; formal analysis, D.C.; investigation, D.C.; resources, D.I.; data curation, D.C.; writing—original draft preparation, D.C.; writing—review and editing, D.C. and D.I.; visualisation, D.C.; supervision, D.I.; project administration, D.I.; funding acquisition, D.I. All authors have read and agreed to the published version of the manuscript.

Funding: This work was partly funded by the European Union's Horizon Europe research and innovation programme through the project LIQUIDICE (grant number: 101184962).

Data Availability Statement: All data processing and analysis code is freely available in the GitHub repository "D_Cyran_Remote_Sensing_Glacier_Albedo" (https://github.com/czawakiach/D_Cyran_Remote_Sensing_Glacier_Albedo (accessed on 23 December 2025), version 1.0). Meteorological data are available through the University of Silesia in Katowice data repository within the Svalbard Integrated Arctic Earth Observing System (SIOS). Landsat 7 imagery is publicly available through the U.S. Geological Survey.

Acknowledgments: Meteorological data have been processed under assessment of the University of Silesia in Katowice data repository within the Svalbard Integrated Arctic Earth Observing System (SIOS). The studies were carried out as part of the scientific activity of the Centre for Polar Studies (University of Silesia in Katowice) with the use of research and logistic equipment (monitoring and measuring equipment, sensors, multiple AWS, snowmobiles, and other supporting equipment) of the Polar Laboratory of the University of Silesia in Katowice. The authors acknowledge the Polish Polar Station Hornsund for logistical support and the Institute of Geophysics, Polish Academy of Sciences, for providing meteorological data. We thank the Landsat program and Google Earth Engine for satellite data access. All data processing and analysis code is freely available in the GitHub repository "D_Cyran_Remote_Sensing_Glacier_Albedo" (https://github.com/czawakiach/D_Cyran_Remote_Sensing_Glacier_Albedo (accessed on 23 December 2025), version 1.0)), enabling full reproducibility of the modelling framework and results. Large Language Models (ChatGPT-3.5, Claude 3.5 Sonnet, Claude 4.0 Sonnet, and Claude 4.5 Sonnet) were used to assist with the code development, debugging, and initial manuscript drafting. All AI-generated content was thoroughly reviewed, verified, and edited by the authors. Final scientific interpretation, analysis, and conclusions are entirely the authors' own work.

Conflicts of Interest: The authors declare no conflicts of interest. The funders had no role in the design of the study; in the collection, analyses, or interpretation of data; in the writing of the manuscript; or in the decision to publish the results.

References

1. Gardner, A.S.; Sharp, M.J. A review of snow and ice albedo and the development of a new physically based broadband albedo parameterization. *J. Geophys. Res. Earth Surf.* **2010**, *115*, F01009. [CrossRef]
2. Cuffey, K.M.; Paterson, W.S.B. *The Physics of Glaciers*, 4th ed.; Academic Press/Elsevier: Amsterdam, The Netherlands, 2010; 704p.
3. Brock, B.W.; Willis, I.C.; Sharp, M.J. Measurement and parameterization of albedo variations at Haut Glacier d'Arolla, Switzerland. *J. Glaciol.* **2000**, *46*, 675–688. [CrossRef]
4. Box, J.E.; Fettweis, X.; Stroeve, J.C.; Tedesco, M.; Hall, D.K.; Steffen, K. Greenland ice sheet albedo feedback: Thermodynamics and atmospheric drivers. *Cryosphere* **2012**, *6*, 821–839. [CrossRef]
5. Tedesco, M.; Doherty, S.; Fettweis, X.; Alexander, P.; Jeyaratnam, J.; Stroeve, J. The darkening of the Greenland ice sheet: Trends, drivers, and projections (1981–2100). *Cryosphere* **2016**, *10*, 477–496. [CrossRef]
6. Naegeli, K.; Huss, M. Sensitivity of mountain glacier mass balance to changes in bare-ice albedo. *Ann. Glaciol.* **2017**, *58*, 119–129. [CrossRef]
7. Stibal, M.; Box, J.E.; Cameron, K.A.; Langen, P.L.; Yallop, M.L.; Mottram, R.H.; Ahlstrøm, A.P. Algae drive enhanced darkening of bare ice on the Greenland ice sheet. *Geophys. Res. Lett.* **2017**, *44*, 11463–11471. [CrossRef]
8. Williamson, C.J.; Cook, J.; Tedstone, A.; Yallop, M.; McCutcheon, J.; Poniecka, E.; Anesio, A.; Irvine-Fynn, T.; McQuaid, J.; Tranter, M.; et al. Algal photophysiology drives darkening and melt of the Greenland Ice Sheet. *Proc. Natl. Acad. Sci. USA* **2020**, *117*, 5694–5705. [CrossRef]
9. Cook, J.M.; Tedstone, A.J.; Williamson, C.; McCutcheon, J.; Hodson, A.J.; Dayal, A.; Tranter, M.; Hofer, S.; Bryant, R.; McAree, O.; et al. Glacier algae accelerate melt rates on the south-western Greenland Ice Sheet. *Cryosphere* **2020**, *14*, 309–330. [CrossRef]
10. Takeuchi, N.; Kohshima, S.; Seko, K. Structure, formation, and darkening process of albedo-reducing material (cryoconite) on a Himalayan glacier: A granular algal mat growing on the glacier. *Arct. Antarct. Alp. Res.* **2001**, *33*, 115–122. [CrossRef]
11. Cook, J.; Edwards, A.; Takeuchi, N.; Irvine-Fynn, T. Cryoconite: The dark biological secret of the cryosphere. *Prog. Phys. Geogr.* **2016**, *40*, 66–111. [CrossRef]
12. van As, D.; Fausto, R.S.; Colgan, W.T.; Box, J.E.; Ahlstrøm, A.P.; Andersen, S.B.; Andersen, M.L.; Charalampidis, C.; Citterio, M.; Edelvang, K.; et al. Darkening of the Greenland ice sheet due to the melt-albedo feedback observed at PROMICE weather stations. *Geol. Surv. Den. Greenl. Bull.* **2013**, *28*, 69–72. [CrossRef]

13. Flanner, M.G.; Zender, C.S. Linking snowpack microphysics and albedo evolution. *J. Geophys. Res. Atmos.* **2006**, *111*, D12208. [CrossRef]
14. Picard, G.; Domine, F.; Krinner, G.; Arnaud, L.; Lefebvre, E. Inhibition of the positive snow-albedo feedback by precipitation in interior Antarctica. *Nat. Clim. Chang.* **2012**, *2*, 795–798. [CrossRef]
15. Xiao, Y.; Ke, C.Q.; Shen, X.; Yu, C.; Li, H. What drives the decrease of glacier surface albedo in High Mountain Asia in the past two decades? *Sci. Total Environ.* **2023**, *863*, 160945. [CrossRef]
16. Draeger, C.; Radić, V.; White, R.H.; Tessema, M.A. Temperature mediated albedo decline portends acceleration of North American glacier mass loss. *Commun. Earth Environ.* **2025**, *6*, 503. [CrossRef]
17. Chen, A.; Wang, L.; Jiao, Y.; Liu, Q.; Yan, M. Observed and projected declines in glacier albedo across the Third Pole in the 21st century. *One Earth* **2024**, *7*, 1481–1495. [CrossRef]
18. Morrison, K.D.; Marsh, C.B.; Onclin, C.; Pomeroy, J.W. Assimilation of satellite albedo to improve simulations of glacier hydrology. *Hydrol. Process.* **2024**, *38*, e15329. [CrossRef]
19. Bolibar, J.; Rabatel, A.; Gouttevin, I.; Galiez, C.; Condom, T.; Sauquet, E. Nonlinear sensitivity of glacier mass balance to future climate change unveiled by deep learning. *Nat. Commun.* **2022**, *13*, 409. [CrossRef]
20. Cook, S.J.; Swift, D.A.; Kirkbride, M.P.; Knight, P.G.; Waller, R.I. Committed ice loss in the European Alps until 2050 using a deep-learning-aided 3D ice-flow model with data assimilation. *Geophys. Res. Lett.* **2023**, *50*, e2023GL105029. [CrossRef]
21. Jouvet, G.; Cordonnier, G.; Kim, B.; Lüthi, M.; Vieli, A.; Bauder, A. A data-consistent model of the last glaciation in the Alps achieved with physics-driven AI. *Nat. Commun.* **2025**, *16*, 168. [CrossRef]
22. Dumont, M.; Gardelle, J.; Sirguey, P.; Guillot, A.; Six, D.; Rabatel, A.; Arnaud, Y. Linking glacier annual mass balance and glacier albedo retrieved from MODIS data. *Cryosphere* **2012**, *6*, 1527–1539. [CrossRef]
23. Greuell, W.; Kohler, J.; Obleitner, F.; Glowacki, P.; Melvold, K.; Bernsen, E.; Oerlemans, J. Assessment of interannual variations in the surface mass balance of 18 Svalbard glaciers from the Moderate Resolution Imaging Spectroradiometer/Terra albedo product. *J. Geophys. Res. Atmos.* **2007**, *112*, D07105. [CrossRef]
24. Oerlemans, J.; Knap, W.H. A 1 year record of global radiation and albedo in the ablation zone of Morteratschgletscher, Switzerland. *J. Glaciol.* **1998**, *44*, 231–238. [CrossRef]
25. van den Broeke, M.; van As, D.; Reijmer, C.; van de Wal, R. Assessing and improving the quality of unattended radiation observations in Antarctica. *J. Atmos. Ocean. Technol.* **2004**, *21*, 1417–1431. [CrossRef]
26. Aas, K.S.; Dunse, T.; Collier, E.; Schuler, T.V.; Berntsen, T.K.; Kohler, J.; Luks, B. The climatic mass balance of Svalbard glaciers: A 10-year simulation with a coupled atmosphere–glacier mass balance model. *Cryosphere* **2016**, *10*, 1089–1104. [CrossRef]
27. Hock, R. Temperature index melt modelling in mountain areas. *J. Hydrol.* **2003**, *282*, 104–115. [CrossRef]
28. Rasp, S.; Pritchard, M.S.; Gentine, P. Deep learning to represent subgrid processes in climate models. *Proc. Natl. Acad. Sci. USA* **2018**, *115*, 9684–9689. [CrossRef]
29. Marshall, S.J.; Sharp, M.J.; Burgess, D.O.; Anslow, F.S. Near-surface-temperature lapse rates on the Prince of Wales Icefield, Ellesmere Island, Canada: Implications for regional downscaling of temperature. *Int. J. Climatol.* **2007**, *27*, 385–398. [CrossRef]
30. Schuler, T.V.; Crochet, P.; Hock, R.; Jackson, M.; Barstad, I. Distribution of snow accumulation on the Svartisen ice cap, Norway, assessed by a model of orographic precipitation. *Hydrol. Process.* **2008**, *22*, 3998–4008. [CrossRef]
31. Naegeli, K.; Huss, M.; Hoelzle, M. Change detection of bare-ice albedo in the Swiss Alps. *Cryosphere* **2019**, *13*, 397–412. [CrossRef]
32. Hock, R.; Holmgren, B. A distributed surface energy-balance model for complex topography and its application to Storglaciären, Sweden. *J. Glaciol.* **2005**, *51*, 25–36. [CrossRef]
33. Łupikasza, E.; Niedźwiedź, T. Long-term variability of precipitation form in Hornsund (Spitsbergen) in relation to atmospheric circulation (1979–2009). *Bull. Geogr. Phys. Geogr. Ser.* **2010**, *3*, 61–72. [CrossRef]
34. Araźny, A.; Migała, K.; Sikora, S.; Budzik, T. Meteorological and biometeorological conditions in the Hornsund area (Spitsbergen) during the warm season. *Pol. Polar Res.* **2010**, *31*, 217–238. [CrossRef]
35. Migała, K.; Nasiołkowski, T.; Pereyma, J. Topoclimatic conditions in the Hornsund area (SW Spitsbergen) during the ablation season 2005. *Pol. Polar Res.* **2008**, *29*, 73–91.
36. Kryza, M.; Szymanowski, M.; Migała, K.; Pietras, M. Spatial information on total solar radiation: Application and evaluation of the r.sun model for the Wedel Jarlsberg Land, Svalbard. *Pol. Polar Res.* **2010**, *31*, 17–32. [CrossRef]
37. Marsz, A.A.; Styszyńska, A. *Climate and Climate Change at Hornsund, Svalbard*; Gdynia Maritime University Press: Gdynia, Poland, 2013.
38. Sikora, S.; Araźny, A.; Budzik, T.; Migała, K.; Puczko, D. Comparison of meteorological conditions in Svalbard fjords: Hornsund and Kongsfjorden. *Oceanologia* **2017**, *59*, 696–708. [CrossRef]
39. Osika, A.; Jania, J. Geomorphological and historical records of the surge-type behaviour of Hansbreen (Svalbard). *Ann. Glaciol.* **2024**, *65*, e31. [CrossRef]
40. Błaszczyk, M.; Luks, B.; Pętlicki, M.; Puczko, D.; Ignatiuk, D.; Laska, M.; Grabiec, M.; Głowacki, P. High temporal resolution records of the velocity of Hansbreen, a tidewater glacier in Svalbard. *Earth Syst. Sci. Data* **2024**, *16*, 1847–1860. [CrossRef]

41. Jania, J.; Mochnacki, D.; Gądek, B. The thermal structure of Hansbreen, a tidewater glacier in southern Spitsbergen, Svalbard. *Polar Res.* **1996**, *15*, 53–66. [CrossRef]
42. Grabiec, M.; Jania, J.A.; Puczko, D.; Kolondra, L.; Budzik, T. Surface and bed morphology of Hansbreen, a tidewater glacier in Spitsbergen. *Pol. Polar Res.* **2012**, *33*, 111–138. [CrossRef]
43. Szafraniec, J. Influence of positive degree-days and sunshine duration on the surface ablation of Hansbreen, Spitsbergen glacier. *Pol. Polar Res.* **2002**, *23*, 227–240.
44. Ignatiuk, D.; Błaszczyk, M.; Budzik, T.; Grabiec, M.; Jania, J.A.; Kondracka, M.; Stachnik, Ł. A decade of glaciological and meteorological observations in the Arctic (Werenskioldbreen, Svalbard). *Earth Syst. Sci. Data* **2022**, *14*, 2487–2507. [CrossRef]
45. Majchrowska, E.; Jania, J.; Ignatiuk, D.; Marszałek, H.; Wąsik, M. Seasonal and interannual variability in runoff from the Werenskioldbreen catchment, Spitsbergen. *Pol. Polar Res.* **2015**, *36*, 197–224. [CrossRef]
46. Błaszczyk, M.; Jania, J.A.; Kolondra, L. Fluctuations of tidewater glaciers in Hornsund Fjord (Southern Svalbard) since the beginning of the 20th century. *Pol. Polar Res.* **2009**, *30*, 407–430. [CrossRef]
47. Błaszczyk, M.; Jania, J.A.; Hagen, J.O. Tidewater glaciers of Svalbard: Recent changes and estimates of calving fluxes. *Pol. Polar Res.* **2009**, *30*, 85–142.
48. *ISO 9060:2018*; Solar Energy—Specification and Classification of Instruments for Measuring Hemispherical Solar and Direct Solar Radiation. International Organization for Standardization: Geneva, Switzerland, 2018.
49. Wawrzyniak, T.; Osuch, M. A 40-year High Arctic climatological dataset of the Polish Polar Station Hornsund (SW Spitsbergen, Svalbard). *Earth Syst. Sci. Data* **2020**, *12*, 805–815. [CrossRef]
50. Osuch, M.; Wawrzyniak, T.; Nawrot, A. Diagnosis of the hydrology of a small Arctic permafrost catchment using HBV conceptual rainfall-runoff model. *Hydrol. Res.* **2017**, *50*, 459–478. [CrossRef]
51. U.S. Geological Survey. *Landsat 7 Enhanced Thematic Mapper Plus (ETM+) Level-1 Data Products*; U.S. Geological Survey: Reston, VA, USA, 2023. Available online: https://www.usgs.gov/landsat-missions/landsat-7 (accessed on 27 September 2024).
52. Gorelick, N.; Hancher, M.; Dixon, M.; Ilyushchenko, S.; Thau, D.; Moore, R. Google Earth Engine: Planetary-scale geospatial analysis for everyone. *Remote Sens. Environ.* **2017**, *202*, 18–27. [CrossRef]
53. Porter, C.; Morin, P.; Howat, I.; Noh, M.J.; Bates, B.; Peterman, K.; Bojesen, M. *ArcticDEM*; Harvard Dataverse: Cambridge, MA, USA, 2018. [CrossRef]
54. Nowak, A.; Hodson, A. Hydrological response of a High-Arctic catchment to changing climate over the past 35 years: A case study of Bayelva watershed, Svalbard. *Polar Res.* **2013**, *32*, 19691. [CrossRef]
55. Pedregosa, F.; Varoquaux, G.; Gramfort, A.; Michel, V.; Thirion, B.; Grisel, O.; Blondel, M.; Prettenhofer, P.; Weiss, R.; Dubourg, V.; et al. Scikit-learn: Machine learning in Python. *J. Mach. Learn. Res.* **2011**, *12*, 2825–2830.
56. Ignatiuk, D. Energy mass balance and temperature-index melt modelling of Werenskioldbreen, Svalbard. *Pol. Polar Res.* **2023**, *44*, 127–152. [CrossRef]
57. Liang, S. Narrowband to broadband conversions of land surface albedo I: Algorithms. *Remote Sens. Environ.* **2001**, *76*, 213–238. [CrossRef]
58. Tasumi, M.; Allen, R.G.; Trezza, R.; Wright, J.L. Satellite-based energy balance to assess within-population variance of crop coefficient curves. *J. Irrig. Drain. Eng.* **2008**, *134*, 441–451. [CrossRef]
59. Silva, B.B.; Braga, A.C.; Braga, C.C.; de Oliveira, L.M.; Montenegro, S.M.; Junior, B.B. Procedures for calculation of the albedo with OLI-Landsat 8 images: Application to the Brazilian semi-arid. *Rev. Bras. Eng. Agríc. Ambient.* **2016**, *20*, 3–8. [CrossRef]
60. Knap, W.H.; Reijmer, C.H.; Oerlemans, J. Narrowband to broadband conversion of Landsat TM glacier albedos. *Int. J. Remote Sens.* **1999**, *20*, 2091–2110. [CrossRef]
61. Williamson, S.N.; Copland, L.; Hik, D.S. The accuracy of satellite-derived albedo for northern alpine and glaciated land covers. *Polar Sci.* **2016**, *10*, 262–269. [CrossRef]
62. Naegeli, K.; Damm, A.; Huss, M.; Wulf, H.; Schaepman, M.; Hoelzle, M. Cross-comparison of albedo products for glacier surfaces derived from airborne and satellite (Sentinel-2 and Landsat 8) optical data. *Remote Sens.* **2017**, *9*, 110. [CrossRef]
63. Schuler, T.V.; Kohler, J.; Elagina, N.; Hagen, J.O.; Hodson, A.J.; Jania, J.A.; Pettersson, R. Reconciling Svalbard glacier mass balance. *Front. Earth Sci.* **2020**, *8*, 156. [CrossRef]
64. Naegeli, K.; Huss, M.; Hoelzle, M. Remote sensing of ice albedo using harmonized Landsat and Sentinel 2 datasets: Validation and inter-comparison of products from Greenland. *Int. J. Remote Sens.* **2024**, *45*, 7724–7752. [CrossRef]

Disclaimer/Publisher's Note: The statements, opinions and data contained in all publications are solely those of the individual author(s) and contributor(s) and not of MDPI and/or the editor(s). MDPI and/or the editor(s) disclaim responsibility for any injury to people or property resulting from any ideas, methods, instructions or products referred to in the content.